Artificial Intelligence in Geosciences 2 (2021) 107–114

Contents lists available at ScienceDirect

Artificial Intelligence in Geosciences

journal homepage: www.keaipublishing.com/en/journals/artificial-intelligence-in-geosciences

# Hydrocarbon detections using multi-attributes based quantum neural networks in a tight sandstone gas reservoir in the Sichuan Basin, China

Ya-juan Xue [a], Xing-jian Wang [b,*], Jun-xing Cao [b], Xiao-Fang Liao [c]

[a] School of Communication Engineering, Chengdu University of Information Technology, Chengdu, 610225, China
[b] State Key Laboratory of Oil and Gas Reservoir Geology and Exploitation, Chengdu University of Technology, Chengdu, 610059, China
[c] College of Geophysics, Chengdu University of Technology, Chengdu, 610059, China

ARTICLE INFO

*Keywords:*
Hydrocarbon detection
Multi-attributes
Quantum neural networks
Tight sandstone gas reservoir
Weak seismic responses

ABSTRACT

A direct hydrocarbon detection is performed by using multi-attributes based quantum neural networks with gas fields. The proposed multi-attributes based quantum neural networks for hydrocarbon detection use data clustering and local wave decomposition based seismic attenuation characteristics, relative wave impedance features of prestack seismic data as the selected multiple attributes for one tight sandstone gas reservoir and further employ principal component analysis combined with quantum neural networks for giving the distinguishing results of the weak responses of the gas reservoir, which is hard to detect by using the conventional technologies. For the seismic data from a tight sandstone gas reservoir in the Sichuan basin, China, we found that multi-attributes based quantum neural networks can effectively capture the weak seismic responses features associated with gas saturation in the gas reservoir. This study is hoped to be useful as an aid for hydrocarbon detections for the gas reservoir with the characteristics of the weak seismic responses by the complement of the multi-attributes based quantum neural networks.

## 1. Introduction

Hydrocarbon detection methods started from the emergence of the bright spot technique in the 1970s which highlights the reflection amplitude changes on the seismic sections and increases the gas layer identification from about 12% to around 60%–80% (Hammond, 1974). It is found that the bright spot technique is more suitable for the gas identification of young, relatively uncompacted sediments in ocean basins than deep deposits below 8000–10000 feet due to the seismic attenuation (Hammond, 1974). In some deep and old strata, the seismic responses of the gas layers on the seismic section may be presented as flat spots or dim spots (Backus and Chen, 1975; Brown, 2012).

AVO analysis is one widely used hydrocarbon detection technique in the recent days (e.g., Wandler et al., 2007; Dupuy and Stovas, 2014; Ismail et al., 2020). The basis of AVO analysis is the Zoeppritz equation that has many expression forms and approximates to mainly reflect the reflection coefficients and the amplitude of the reflection wave which is a complex function of the incident angle and the physical parameters on both sides of the reflection interface (e.g., Aki and Richards, 1980; Shuey, 1985; Castagna and Backus, 1993a; Fatti et al., 1994). From the different approximates of the Zoeppritz equation, many types of pre-stack seismic inversion methods are developed to obtain many physical parameters such as longitudinal and transverse waves' velocity and density, Poisson's ratio, and relative wave impedance for hydrocarbon detections (Castagna and Backus, 1993b; Pan et al., 1994; Tetyukhina et al., 2014; Cao et al., 2021). Although AVO analysis has a rigorous mathematical foundation, there are many assumptions in practice applications, and the current successful application cases are basically clastic rock reservoirs with shallow burial.

Seismic attenuation estimation methods are another widely used techniques which use the energy attenuation characteristics of seismic waves for reservoir characterization and hydrocarbon detection (e.g., Mitchell et al., 1996; Partyka et al., 1999; Castagna et al., 2003; Sinha et al., 2005; Xue et al., 2016a; Wang et al., 2019). Laboratory experiments and field data measurements show that seismic wave attenuated more pronouncedly for viscous fluid-saturated rocks than dry rocks in most frequency bandwidths and the high-frequency components of seismic waves are attenuated more rapidly than the low-frequency components in gas-prone sediments (Domenico, 1974; Anderson and Hampton, 1980; Dvorkin and Nur, 1993; del Valle-García and Ramírez-Cruz, 2002; Korneev et al., 2004; Xue et al., 2019). Strong amplitude anomalies of seismic waves at specific frequencies can be easily found

* Corresponding author.
*E-mail addresses:* xueyj0869@163.com (Y.-j. Xue), wangxj@cdut.edu.cn (X.-j. Wang).

https://doi.org/10.1016/j.aiig.2022.02.004
Received 1 January 2022; Received in revised form 23 February 2022; Accepted 24 February 2022
Available online 26 February 2022

through the seismic attenuation estimation methods such as spectrum decomposition (e.g., Castagna et al., 2003; Korneev et al., 2004; Sinha et al., 2005; Duchesne et al., 2011) and attenuation gradient estimation (e.g., Mitchell et al., 1996; Pramanik et al., 2000; del Valle-García and Ramírez-Cruz 2002; Xue et al., 2016a). Seismic attenuation estimation technology mainly uses the time-frequency methods to estimate the attenuation. The conventional time-frequency methods including the short-time Fourier transform, wavelet transform, Wigner-ville distribution are always limited by the Heisenberg/Gabor uncertainty principle and cannot have a high resolution at time and frequency simultaneously (Gabor, 1946). The recent local wave decomposition based high-resolution time-frequency methods including the Hilbert-huang transform, scynchrosqueezed transforms show much higher time-frequency resolution than the conventional time-frequency methods, but the narrow frequency band properties of these methods are the major challenge for seismic interpretation (Xue et al., 2019).

In recent days, machine learning (ML) methods are also used for delineate reservoirs by the formulation of fluid and rock properties of gas reservoirs to a set of predefined seismic attributes (Chaki et al., 2018; Kadkhodaie and Kadkhodaie, 2022). Artificial neural network (ANN) is used to build models for reservoir permeability prediction (Zolotukhin and Gayubov, 2019; Tian et al., 2021). Tahmasebi et al. (2017) combined the fuzzy logic approach with neural networks and the genetic algorithm for predicting the total organic carbon and fracable index in shale reservoirs. Wang et al. (2020) utilized fuzzy self-organizing map and the radial basis function neural network for spectral attributes generated from principal component analysis of the common frequency sections to estimate reservoir thickness. The Support Vector Machine (SVM) and relevant vector machine are verified to have better performance in most cases than the ANN with different shallow models due to an improved parameter selection in reservoir characterization (Otchere et al., 2021). Delavar (2022) applied the hybrid SVM and grey wolf optimizer methods for fracture classification in carbonate reservoirs. Long Short-Term Memory is used to build a prediction model for water saturation prediction (Zhang et al., 2019). Singh et al. (2021) comparatively studied 12 different ML algorithms, which belong to the classes of ridge regression and its variants, decision tree and its variants, k-nearest neighbour, reduced order models and neural network, for predicting gas hydrate saturation. However, it is difficult to find a single ML method working for all the reservoirs due to the different lithology and geology.

In this paper, for enhancing the approximation and information processing efficiency of conventional neural networks, we attempt to use quantum neural networks to extract the features from the integration of data clustering results, local wave decomposition based seismic attenuation, relative wave impedance attributes of pre-stack seismic data, and give the distinguishing results of the weak gas responses in one tight sandstone gas reservoir in the Sichuan basin, China, which is hard to detect by using the conventional technologies.

## 2. Materials and methods

### 2.1. Seismic data

The prestack seismic data from the gas field in one tight sandstone gas reservoir in the Sichuan basin, China, is collected. The reservoir which is mainly the multi-phase multi-stacked Delta plain and Delta front dominated river sand body has the characteristics of strong heterogeneity, low porosity and permeability (Li et al., 2016; Lu et al., 2019). The physical properties difference between sandstone and mudstone in the work area is small. Some sand bodies which belong to the hidden river sands are very thin. The seismic response is weak (Tan et al., 2021), and gas detection in the reservoir especially for the non-bright spot channels is difficult.

Here, six well logging data and the corresponding seismic traces intersecting the known wells are used for training the quantum gate set neural network (QGSNN). According to the well interpretations, the gas reservoirs are divided into four types: strong gas layer, poor gas layer, gas and water layer, hidden reservoirs. Hydrocarbon detections for two seismic sections intersecting the known wells named A and B are analysed in detail. The seismic signals are sampled at 1 ms. The far (incident angle ranges from 29° to 40°) and near (incident angle ranges from 0° to 13°) offset trace stacked profiles are used for hydrocarbon detection.

### 2.2. Quantum neural networks

Quantum neural network (QNN) which combines the basics of ANN with quantum computation paradigm can better simulate the information processing procedure in the human brain and enhance approximation and information processing efficiency of neural networks (Kak, 1995; Menneer, 1998; Behrman et al., 1999; Ezhov and Ventura, 2000; Matsui et al., 2009; Kouda et al., 2003; Schuld et al., 2014). Currently, it has been successfully applied to fields such as image processing, pattern recognition, handwritten characters recognition (e.g., Masato et al., 2000; Ren et al., 2010; Mu et al., 2013). Till date there are various types of QNN model (Jeswal and Chakraverty, 2019). In this paper, we adopt a QGSNNfor hydrocarbon detection.

QGSNN is a combination of several universal quantum gates in accordance with a certain topology. A three-layer neural network structure including the input layer, the hidden layer, and the output layer is adopted in this paper. In QGSNN model (Fig. 1), the input is $|x_i>,(i=1,2,\cdots n)$, and $\theta$ is the connection weight between the input layer and the hidden layer. The output of hidden layer is $|h_j>,(j=1,2,\cdots p)$, and $\varphi$ is the connection weight between the hidden layer and the output layer. The network output is $|y_k>,(k=1,2,\cdots,m)$.Let

$$|x_i\rangle=\cos\theta_i|0\rangle+\sin\theta_i|1\rangle, \tag{1}$$

the output of hidden layer is

$$\left|h_j>=\cos(\varphi_j)\right|0>+\prod_{i=1}^{n}\sin(\theta_i+\theta_{ij})\left|1>=\cos(\varphi_j)\right|0>+\sin(\varphi_j)\left|1>, \tag{2}$$

and the network output is

$$\left|y_k>=\cos(\xi_k)\right|0>+\prod_{j=1}^{p}\sin(\varphi_j+\varphi_{jk})\left|1>=\cos(\xi_k)\right|0>+\sin(\xi_k)\left|1>, \tag{3}$$

in which $\varphi_j=\arcsin(\prod_{i=1}^{n}\sin(\theta_i+\theta_{ij}))$, $\xi_k=\arcsin(\prod_{j=1}^{p}\sin(\varphi_j+\varphi_{jk}))$.

### 2.3. Hydrocarbon detection using multi-attributes fusion based quantum neural networks

Different seismic attributes may reflect the different information of the seismic data related to the structure, stratigraphy, lithology and hydrocarbons. For a specific gas reservoir, the seismic attributes should be selected carefully according to the sensitivity of different work areas and different reservoirs to the seismic attributes of the predicted objects. In seismic attributes, the relative wave impedance features may reflect the lithological changes. The local wave decomposition based seismic attenuation characteristics are related to the hydrocarbon contents. Data clustering results of prestack seismic data are the sum of the appearances of sedimentary facies on a seismic section to a certain degree, and they represent the lithological assemblage, bedding, and sedimentary characteristics of the sediments that give rise to its reflections. Therefore, for effectively distinguishing the weak responses of the gas reservoir, we mainly select the relative wave impedance features, the local wave decomposition based seismic attenuation characteristics and data clustering results of prestack seismic data as the featured seismic attributes

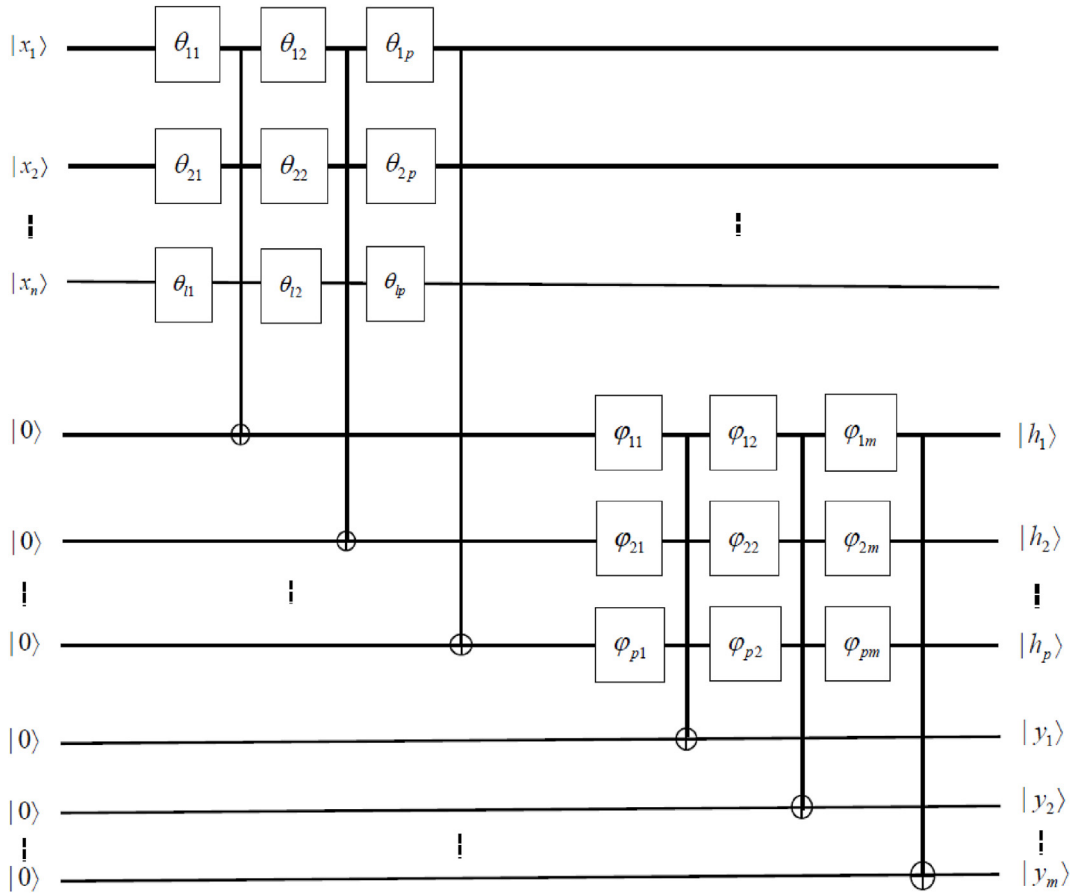


**Fig. 1.** QGSNN model. The input is $|x_i>, (i = 1, 2, \cdots n)$, and $\theta$ is the connection weight between the input layer and the hidden layer. The output of hidden layer is $|h_j>, (j = 1, 2, \cdots p)$, and $\varphi$ is the connection weight between the hidden layer and the output layer. The network output is $|y_k>, (k = 1, 2, \cdots, m)$.

for training the QGSNN. Relative seismic impedances of the far and near offset trace stacked profiles are extracted at first. For the local wave decomposition based seismic attenuation estimation, we mainly select the CEEMD-based attenuation gradient estimation method ((Xue et al., 2016a) and the wavelet-based cepstrum decomposition method (Xue et al., 2016b). Based on the difference volume between the far and near offset trace stacked profiles, we extract the difference volume between the first-order and second-order of the wavelet-based cepstrum, and the CEEMD-based attenuation gradient volume. Seismic data clustering using Self-Organization Map (SOM) neural network for the difference profile is also used. Principal component analysis (PCA) is then used to these seismic attributes to decrease the data dimension. Subsequently, for the obtained principal components, we transform them into quantum state representations. Assume the seismic attributes set being $\overline{X} = (\overline{x}_1, \overline{x}_2, \cdots, \overline{x}_n)^T$, $(\overline{x}_i \in [a_i, b_i])$, in which $\overline{x}_i$ denotes one seismic attribute in its ranges from $a_i$ to $b_i$. Now let $\theta_i = \frac{2\pi(\overline{x}_i - a_i)}{b_i - a_i}$, and the quantum state of $\overline{X}$ is set by

$$|X\rangle = [|x_1\rangle, |x_2\rangle, \cdots, |x_n\rangle]^T, \tag{4}$$

in which $|x_i\rangle = [\cos\theta_i \ \ \sin\theta_i]^T$.

Taken the probability amplitude of the quantum state $|1\rangle$ in each layer as the actual output of each layer, the actual output of the hidden layer is obtained as

$$h_j = \sin(\varphi_j) = \prod_{i=1}^{n} \sin(\theta_i + \theta_{ij}), \tag{5}$$

and the actual output of the network is

$$y_k = \prod_{j=1}^{p} \sin(\varphi_j + \varphi_{jk}) = \prod_{j=1}^{p} \sin\left(\arcsin\left(\prod_{i=1}^{l} \sin(\theta_i + \theta_{ij})\right) + \varphi_{jk}\right). \tag{6}$$

Next, the error value of the neural network is calculated, and an error reverse propagation calculation is performed to adjust the network layer parameters. The error value of the neural network is defined as

$$E = \frac{1}{2}\sum_{k=1}^{m} (\tilde{y}_k - y_k)^2, \tag{7}$$

where $\tilde{y}_k$ is the expectant output.

Since there is a large number of minimum values in the quantum neural network, in order to improve the search effects, the particle swarm optimization (PSO) is used to calculate the bias matrices $\theta$ of the hidden layer and $\varphi$ of the network output layer in the quantum neural network. The global search method is used to optimize the parameters of the QGSNN. Furthermore, based on the global search, gradient decreased method is employed to find the optimal solution of the bias matrices $\theta$ of the hidden layer and $\varphi$ of the network output layer in the quantum neural network for decreasing the network error continuously. According to the gradient decreased method, the update of the rotation angle of each layer is

$$\theta_{ij}(t+1) = \theta_{ij}(t) - \eta\frac{\partial E}{\partial \theta_{ij}}, \tag{8}$$

$$\varphi_{jk}(t+1) = \varphi_{jk}(t) - \eta\frac{\partial E}{\partial \varphi_{jk}}, \tag{9}$$

where $\eta$ is learning rate, and $t$ is the iterative step. The gradient of the

rotation angle of each layer is

$$-\frac{\partial E}{\partial \theta_{ij}} = \sum_{k=1}^{m}(\bar{y}_k - y_k)y_k \cot(\varphi_j + \varphi_{jk})h_j \cot(\theta_i + \theta_{ij}) \Big/ \sqrt{1-h_j^2}, \tag{10}$$

$$-\frac{\partial E}{\partial \varphi_{jk}} = (\bar{y}_k - y_k)y_k \cot(\varphi_j + \varphi_{jk}). \tag{11}$$

After we get the trained parameters $\{\theta,\varphi,E_{final}\}$, in which $E_{final}$ denotes the final $E$, hydrocarbon detections for the seismic sections are carried out by using these trained parameters. The workflow of the multi-attributes fusion based quantum neural networks is shown in Fig. 2.

## 3. Results and discussion

### 3.1. Results

The search effects of the PSO and the QGSNN are respectively shown in Figs. 3 and 4. The near and far offset trace stacked sections intersecting well A are shown in Fig. 5. Different seismic attributes for seismic sections intersecting well A are shown in Fig. 6. A comparison results of the QGSNN and the conventional BP for hydrocarbon detection are shown in Fig. 7. Note that the same workflow as in Fig. 2 is used here to replace the QGSNN with the BP. For further testing the proposed method, analysis on the near and far offset trace stacked sections intersecting well B (Fig. 8a and b) is also given in detail. Different seismic attributes for seismic sections intersecting well B are shown in Fig. 8c~h. The comparison results of the QGSNN and the conventional BP for hydrocarbon detection for section intersecting well B are shown in Fig. 9.

### 3.2. Data analysis

#### 3.2.1. Searching performance of the QGSNN

The parameters used in our multi-attributes fusion based QGSNN workflow are as follows: number of hidden neurons:10; The maximum number of iterations:10000; number of particle swarm:40; particle maximum flight speed:1; maximum iteration step of particle swarm:200; learning rate: 0.01.

Here, we take the seismic sections intersecting well A for analysing the searching performance of the QGSNN. As Fig. 3 shows, the variance of the minimum error of neural networks got by the PSO is 39.2. The PSO gives the global optimal values of the bias matrices $\theta$ of the hidden layer and $\varphi$ of the network output layer. The QGSNN further gives the local optimal values of the bias matrices $\theta$ of the hidden layer and $\varphi$ of the network output layer (Fig. 4). As Fig. 4 shows, the error variance after neural network training by the gradient decreased method is 36.2. Combined with the PSO, the error variance of the QGSNN is further decreased, and the search effects are improved.

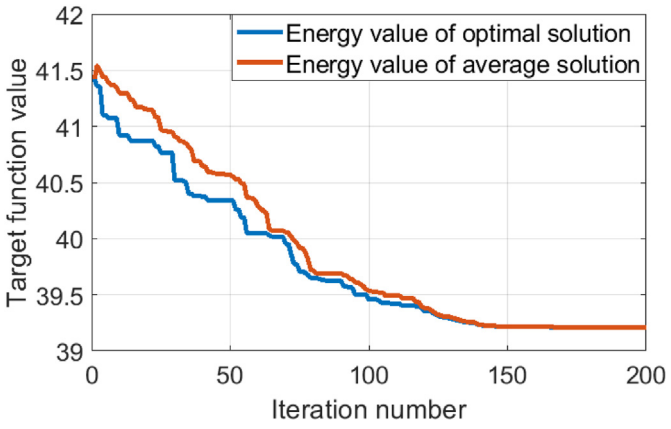


**Fig. 3.** The search effects of PSO.

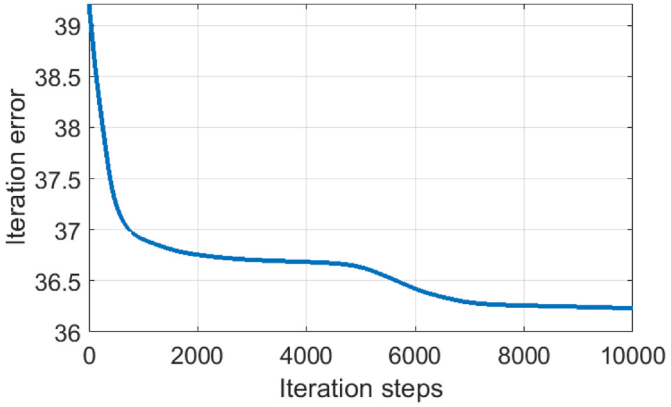


**Fig. 4.** The search effects of QGSNN.

#### 3.2.2. Seismic attributes analysis

For seismic sections intersecting well A, as shown in Fig. 5, there are weak seismic responses existed at the gas area between the horizontal lines H1 and H2, and strong seismic responses existed at the poor gas, gas and water area between the horizontal lines H3 and H4. Fig. 6 shows the different seismic attributes volumes. From Fig. 6 one can find that in the difference section between the far and near offset trace stacked sections intersecting well A (Fig. 6a), the weak seismic responses existed at the gas area between the horizontal lines H1 and H2 are enhanced. Data clustering results (Fig. 6b) show that there are some different data characteristics for the two reservoir areas. The areas where poor gas, gas and water are located have more data clustering types than the weak responses-exhibited gas area. Relative seismic impedances of the near

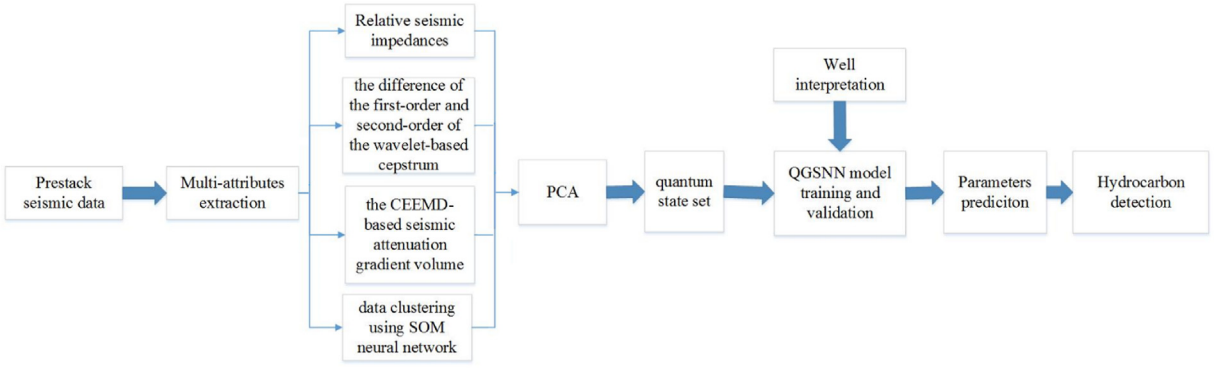


**Fig. 2.** The workflow of the multi-attributes based quantum neural networks.

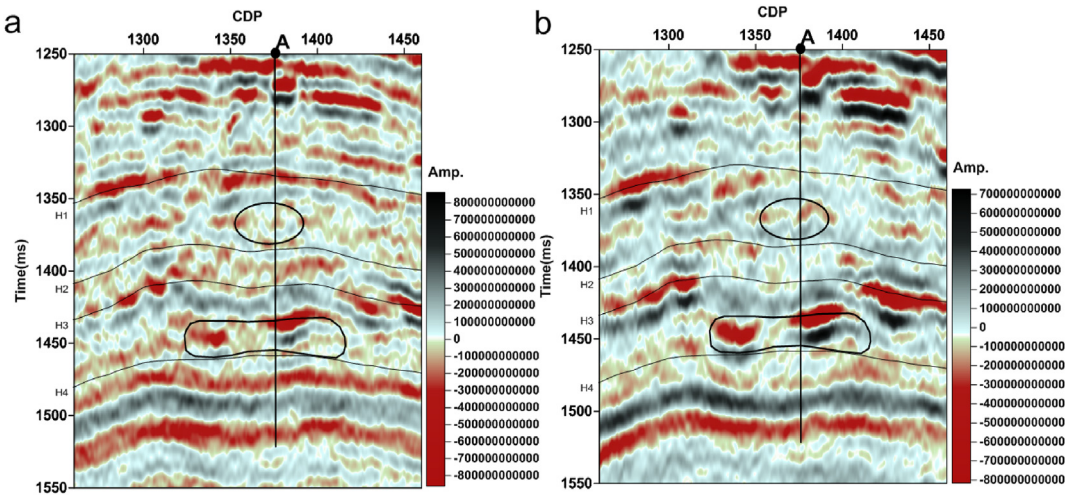


**Fig. 5.** The near (a) and far (b) offset trace stacked sections intersecting well A.

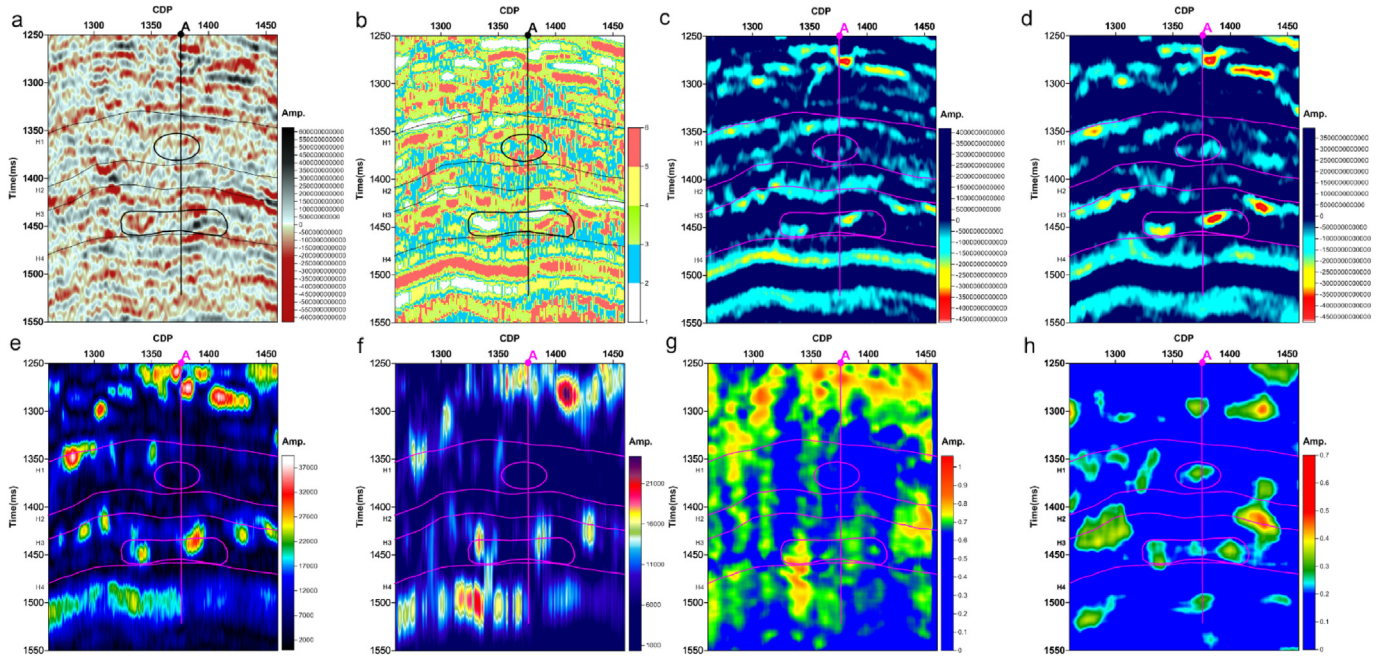


**Fig. 6.** Different seismic attributes for seismic sections intersecting well A. a. the difference volume between the far and near offset trace stacked profiles. b. Data clustering volume for the difference volume in a. c. Relative seismic impedances of the near offset trace stacked profiles. d. Relative seismic impedances of the far offset trace stacked profiles. e. the instantaneous amplitude volume for the difference volume in a. f. the peak amplitude volume above the average for the difference volume in a. g. the CEEMD-based attenuation gradient volume for the difference volume in a. h. the difference section between the first-order and second-order of the wavelet-based cepstrum for the difference volume in a.

and far offset trace stacked profiles (Fig. 6c and d) show there are relatively low values existed at the area where poor gas, gas and water are located and medium amplitudes existed at the weak responses-exhibited gas area. The instantaneous amplitude volume (Fig. 6e) and the peak amplitude volume above the average (Fig. 6f) show there are larger amplitudes existed in the areas where poor gas, gas and water are located, and no obvious amplitude anomalies in the weak responses-exhibited gas area. The CEEMD-based attenuation gradient volume (Fig. 6g) gives the similar interpretation results and it only detects the reservoir located at the poor gas, gas and water bearing areas. The difference section between the first-order and second-order of the wavelet-based cepstrum (Fig. 6h) shows there are obvious amplitude anomalies existed in the weak responses-exhibited gas area and the areas where poor gas, gas and water are located. As Fig. 6 shows, we can find that there is not one seismic attribute which can gives the accurate hydrocarbon-prone interpretation especially for the weak responses-exhibited gas area. Therefore, according the different detection ability of the different seismic attributes, we mainly select the data clustering volume, relative seismic impedances of the near and far offset trace stacked profiles, the CEEMD-based seismic attenuation gradient volume and the difference section between the first-order and second-order of the wavelet-based cepstrum for further hydrocarbon detection using QGSNN.

The selected attributes are further used for another near and far offset trace stacked sections intersecting well B (Fig. 8a and b). There are three gas areas located between the horizontal lines H3 and H4. Stronger reflection amplitudes are mainly existed at the third reservoir area marked by the pink ellipse, and weak seismic responses are found at the

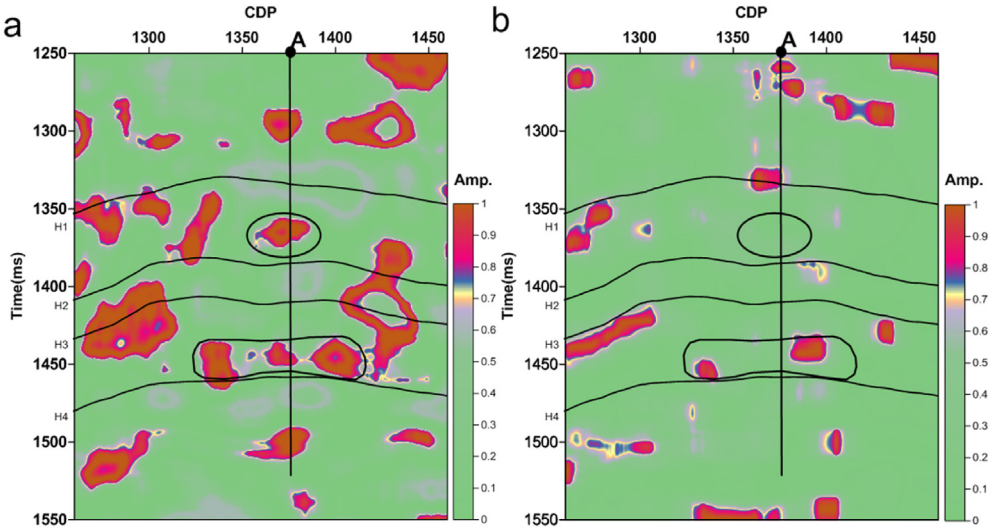


**Fig. 7.** Hydrocarbon detection results for seismic section intersecting well A using the different methods. (a) QGSNN. (b) BP.

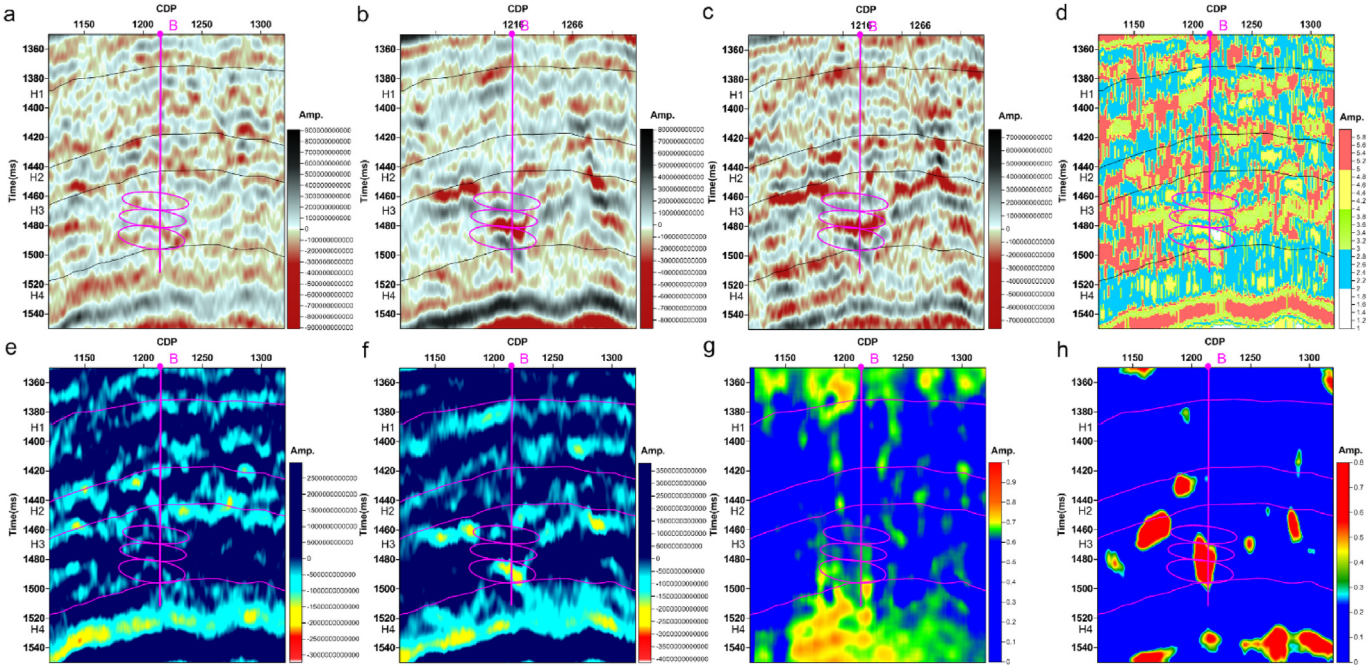


**Fig. 8.** Different seismic attributes for seismic sections intersecting well B. a. the near offset trace stacked profiles. b. the far offset trace stacked profiles. c. the difference volume between the far and near offset trace stacked profiles. d. Data clustering volume for the difference volume in a. e. Relative seismic impedances of the near offset trace stacked profiles. f. Relative seismic impedances of the far offset trace stacked profiles. g. the CEEMD-based attenuation gradient volume for the difference volume in a. h. the difference section between the first-order and second-order of the wavelet-based cepstrum for the difference volume in a.

first and second reservoir areas marked by the pink ellipses. Fig. 8c~h shows the selected seismic attributes for further QGSNN prediction. The selected data clustering volume (Fig. 8d) shows that there are different data characteristics existed for the three gas-bearing areas. The relative seismic impedances of the near and far offset trace stacked profiles (Fig. 8e and f) show that relatively low values are existed for the first and third gas-bearing areas, and no obvious characteristics can be found in the second gas-bearing area. The CEEMD-based seismic attenuation gradient volume (Fig. 8g) shows that there are some little stronger amplitude anomalies existed in the three gas-bearing areas. The difference section between the first-order and second-order of the wavelet-based cepstrum (Fig. 8h) targets the gas reservoir well but it cannot distinguish the different reservoirs. Therefore, when the PCA results of these selected seismic attributes are used, the main contributor components will be used for further improving the hydrocarbon detections using QGSNN.

### 3.2.3. *Hydrocarbon detection*

For hydrocarbon detection for seismic section intersecting well A, we can find that most conventional seismic attributes (Fig. 6) are unable to give a gas-prone interpretation for the weak responses-exhibited gas area located between the horizontal lines H1 and H2. For improving the hydrocarbon detection ability, PCA combined with QGSNN are used for hydrocarbon detection. As Fig. 7a shows, strong amplitude anomalies are existed in the weak responses-exhibited gas area between H1 and H2 and the areas where poor gas, gas and water are located between H3 and H4. QGSNN targets the reservoir accurately and gives a good hydrocarbon-prone interpretation. Compared with the conventional BP method, the

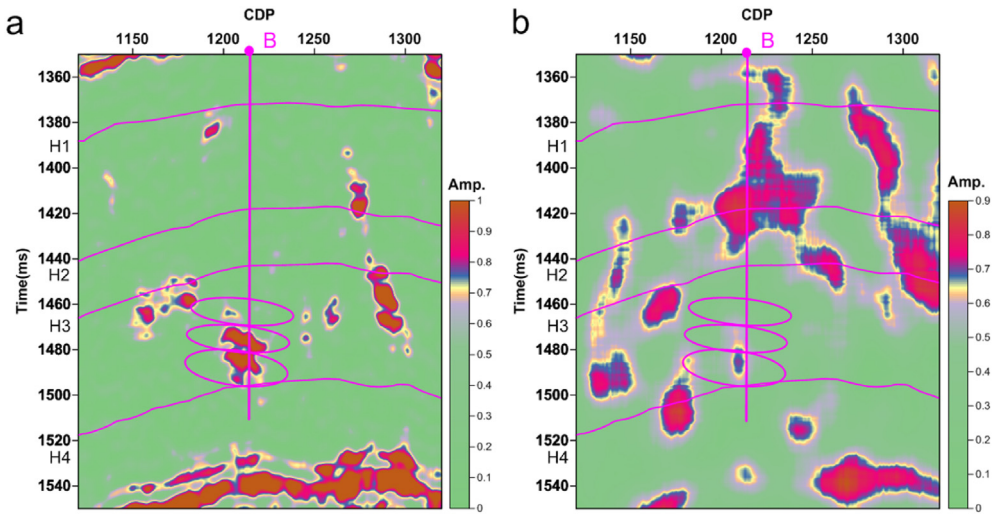


**Fig. 9.** Hydrocarbon detection results for seismic section intersecting well B using the different methods. (a) QGSNN. (b) BP.

hydrocarbon detection ability especially for the weak responses-exhibited gas area is highly improved by using QGSNN.

For further testing the ability of the multi-attributes based QGSNN, the seismic sections intersecting well B are used. Based on the selected seismic attributes volumes (Fig. 8), the PSO-assisted QGSNN combined with PCA is applied (Fig. 9a). A bit strong amplitude anomaly is found in the first gas-bearing area marked by the pink ellipse, and strong amplitude anomalies are found in the second and third gas-bearing areas marked by the pink ellipses. The hydrocarbon detection using the conventional BP method is also given in Fig. 9b. Strong amplitude anomalies can be found at the area near the well B between the horizontal lines H1 and H3 where there is no gas production. Compared with the conventional BP method, the QGSNN targets the reservoirs more accurately and gives the distinguished interpretation results for the three gas-bearing areas.

## 4. Conclusions

Hydrocarbon detection using a multi-attributes based quantum neural network for a tight sandstone gas reservoir in the Sichuan Basin, China is mainly studied in this paper. For hydrocarbon detections, the relative wave impedance features, the local wave decomposition based seismic attenuation characteristics and data clustering results of prestack seismic data are selected as the featured seismic attributes. For the local wave decomposition based seismic attenuation characteristics, the CEEMD-based attenuation gradient estimation method and the wavelet-based cepstrum decomposition method are mainly used. Combined with PCA of the selected featured seismic attributes, the PSO-assisted QGSNN is applied to the data acquired from the tight sandstone gas reservoir in the Sichuan Basis. Application results show that the proposed method is capable for detecting the weak responses-exhibited gas area where the seismic attributes and the conventional BP methods give the poor gas-prone interpretations.

## Declaration of competing interest

The authors declare that they have no known competing financial interests or personal relationships that could have appeared to influence the work reported in this paper.

## Acknowledgments

The research is supported in part by the Central Government Funds of Guiding Local Scientific and Technological Development for Sichuan Province (No. 2021ZYD0030), and in part by the National Natural Science Foundation of China (Nos. 41804140, 42074163, 41974160, 42030812).

## Appendix A. Supplementary data

Supplementary data to this article can be found online at https://doi.org/10.1016/j.aiig.2022.02.004.

## References

Anderson, A.L., Hampton, L.D., 1980. Acoustics of gas-bearing sediments I. Background. J. Acoust. Soc. Am. 67 (6), 1865–1889.
Aki, K., Richards, P.G., 1980. Quantitative Seismology, Theory and Methods. W.H. Freeman and Co, San Francisco, pp. 147–148.
Backus, M.M., Chen, R.L., 1975. Flat spot exploration. Geophys. Prospect. 23 (3), 533–577.
Behrman, E.C., Steck, J.E., Skinner, S.R., 1999. A spatial quantum neural computer. Proc. Int. Joint Conf. Neural Network 2, 874–877.
Brown, A.R., 2012. Dim spots: opportunity for future hydrocarbon discoveries? Lead. Edge 31 (6), 682–683.
Cao, D., Su, Y., Cui, R., 2021. Multi-parameter pre-stack seismic inversion based on deep learning with sparse reflection coefficient constraints. J. Petrol. Sci. Eng. 109836.
Castagna, J.P., Backus, M.M., 1993a. AVO analysis—tutorial and review. In: Offset-dependent reflectivity—Theory and practice of AVO analysis: SEG Investigations in Geophysics, 8, pp. 3–36.
Castagna, J.P., Backus, M.M., 1993b. Offset-dependent Reflectivity—Theory and Practice of AVO Analysis. Society of Exploration Geophysicists, Tulsa, pp. 287–332.
Castagna, J.P., Sun, S., Siegfried, R.W., 2003. Instantaneous spectral analysis: detection of low-frequency shadows associated with hydrocarbons. Lead. Edge 22 (2), 120–127.
Chaki, S., Routray, A., Mohanty, W.K., 2018. Well-log and seismic data integration for reservoir characterization: a signal processing and machine-learning perspective. IEEE Signal Process. Mag. 35 (2), 72–81.
del Valle-García, R., Ramírez-Cruz, L., 2002. Spectral attributes for attenuation analysis in a fractured carbonate reservoir. Lead. Edge 21 (10), 1038–1041.
Delavar, M.R., 2022. Hybrid machine learning approaches for classification and detection of fractures in carbonate reservoir. J. Petrol. Sci. Eng. 208, 109327.
Domenico, S.N., 1974. Effect of water saturation on seismic reflectivity of sand reservoirs encased in shale. Geophysics 39 (6), 759–769.
Duchesne, M.J., Halliday, E.J., Barrie, J.V., 2011. Analyzing seismic imagery in the time–amplitude and time–frequency domains to determine fluid nature and migration pathways: a case study from the Queen Charlotte Basin, offshore British Columbia. J. Appl. Geophys. 73 (2), 111–120.
Dupuy, B., Stovas, A., 2014. Influence of frequency and saturation on AVO attributes for patchy saturated rocks. Geophysics 79 (1), B19–B36.
Dvorkin, J., Nur, A., 1993. Dynamic poroelasticity: a unified model with the squirt and the Biot mechanisms. Geophysics 58 (4), 524–533.
Ezhov, A.A., Ventura, D., 2000. Quantum neural networks. In: Kasabov, N. (Ed.), Future Directions for Intelligent Systems and Information Sciences. Physica, Heidelberg, pp. 213–235.
Fatti, J.L., Smith, G.C., Vail, P.J., Strauss, P.J., Levitt, P.R., 1994. Detection of gas in sandstone reservoirs using AVO analysis: a 3-D seismic case history using the Geostack technique. Geophysics 59 (9), 1362–1376.
Gabor, D., 1946. Theory of communication. J. Inst. Eng. Electron. 93 (26), 429–457.

Hammond, A.L., 1974. Bright spot: better seismological indicators of gas and oil. Science 185 (4150), 515–517.
Ismail, A., Ewida, H.F., Al-Ibiary, M.G., et al., 2020. Application of AVO attributes for gas channels identification, West offshore Nile Delta, Egypt. Petrol. Res. 5 (2), 112–123.
Jeswal, S.K., Chakraverty, S., 2019. Recent developments and applications in quantum neural network: a review. Arch. Comput. Methods Eng. 26 (4), 793–807.
Kadkhodaie, A., Kadkhodaie, R., 2022. Acoustic, density, and seismic attribute analysis to aid gas detection and delineation of reservoir properties. Sustain. Geosci. Nat. Gas Subsurface Sys. 51–92.
Kak, S.C., 1995. On quantum neural computing. Inf. Sci. 83, 143–160.
Kouda, N., Matsui, N., Nishimura, H., Peper, F., 2003. Qubit neural network and its efficiency. Int. Conferen. Knowledge-Based Intel. Inform. Eng. Sys. 304–310.
Korneev, V.A., Goloshubin, G.M., Daley, T.M., Silin, D.B., 2004. Seismic low-frequency effects in monitoring fluid-saturated reservoirs. Geophysics 69 (2), 522–532.
Li, Z., Ran, L., Li, H., Liu, F., Zhou, W., Xiang, Y., 2016. Fault features and enrichment laws of narrow-channel distal tight sandstone gas reservoirs: a case study of the Jurassic Shaximiao Fm gas reservoir in the Zhongjiang Gas Field, Sichuan basin. Nat. Gas. Ind. B 3 (5), 409–417.
Lu, B.P., L, U., Ding, S.D., He, L., Pang, W., 2019. Key achievement of drilling & completion technologies for the efficient development of low permeability oil and gas reservoirs. Petrol. Drill. Techn. 1, 2019.
Masato, T., Nobuyuki, M., Haruhiko, N., 2000. Learning performance of neuron model based on quantum superposition. In: Proceedings of the 9th IEEE International Workshop on Robot and Human Interactive Communication,Osaka,Japan, pp. 112–117.
Matsui, N., Nishimura, H., Isokawa, T., 2009. Qubit neural networks: its performance and applications. In: Nitta, T. (Ed.), Complex-valued Neural Networks: Utilizing High-Dimensional Parameters, Information Science Reference. IGI Global, Hershey, pp. 325–351.
Menneer, T., 1998. Quantum Artificial Neural Networks. PhD thesis. University of Exeter.
Mitchell, J.T., Derzhi, N., Lichma, E., 1996. Energy Absorption Analysis: A Case Study. Expanded Abstracts of 66th Annual Internat SEG Mtg, pp. 1785–1788.
Mu, D., Guan, Z., Zhang, H., 2013. Learning algorithm and application of quantum neural networks with quantum weights. Int. J. Comp. Theory Eng. 5 (5), 788–792.
Otchere, D.A., Ganat, T.O.A., Gholami, R., Ridha, S., 2021. Application of supervised machine learning paradigms in the prediction of petroleum reservoir properties: comparative analysis of ANN and SVM models. J. Petrol. Sci. Eng. 200, 108182.
Pan, G.S., Young, C.Y., Castagna, J.P., 1994. An integrated target-oriented prestack elastic waveform inversion: sensitivity, calibration, and application. Geophysics 59 (9), 1392–1404.
Partyka, G., Gridley, J., Lopez, J., 1999. Interpretational applications of spectral decomposition in reservoir characterization. Lead. Edge 18 (3), 353–360.
Pramanik, A.G., Singh, V., Dubey, A.K., Painuly, P.K., Sinha, D.P., 2000, August. Estimation of Q from borehole data and its application to enhance surface seismic resolution: a case study. In: 2000 SEG Annual Meeting. OnePetro.
Ren, X., Zhang, F., Zheng, L., Men, X., 2010. Application of quantum neural network based on rough set in transformer fault diagnosis. In: 2010 IEEE Asia-Pacific Power and Energy Engineering Conference, pp. 1–4.
Schuld, M., Sinayskiy, I., Petruccione, F., 2014. The quest for a quantum neural network. Quant. Inf. Process. 13 (11), 2567–2586.
Singh, H., Seol, Y., Myshakin, E.M., 2021. Prediction of gas hydrate saturation using machine learning and optimal set of well-logs. Comput. Geosci. 25 (1), 267–283.
Sinha, S., Routh, P.S., Anno, P.D., et al., 2005. Spectral decomposition of seismic data with continuous-wavelet transform. Geophysics 70 (6), P19–P25.
Shuey, R.T., 1985. A simplification of the Zoeppritz equations. Geophysics 50 (4), 609–614.
Tan, F., Cao, J.X., Wang, X.J., Bai, P., Liu, J., You, J.C., 2021. Amplitude variation with offset analysis of nonbright spots for gas channel identification: a case study from the western Sichuan Basin, China. Interpretation 9 (4), T1129–T1137.
Tahmasebi, P., Javadpour, F., Sahimi, M., 2017. Data mining and machine learning for identifying sweet spots in shale reservoirs. Expert Syst. Appl. 88, 435–447.
Tetyukhina, D., Luthi, S.M., Gisolf, D., 2014. Acoustic nonlinear full-waveform inversion on an outcrop-based detailed geological and petrophysical model (Book Cliffs, Utah). AAPG (Am. Assoc. Pet. Geol.) Bull. 98 (1), 119–134.
Tian, J., Qi, C., Sun, Y., Yaseen, Z.M., Pham, B.T., 2021. Permeability prediction of porous media using a combination of computational fluid dynamics and hybrid machine learning methods. Eng. Comput. 37 (4), 3455–3471.
Wandler, A., Evans, B., Link, C., 2007. AVO as a fluid indicator: a physical modeling study. Geophysics 72 (1), C9–C17.
Wang, Xing-jian, Xue, Ya-juan, Zhou, Wen, Luo, Jun-song, 2019. Spectral decomposition of seismic data with a variational mode decomposition-based Wigner-Ville distribution. IEEE J. Sel. Top. Appl. Earth Obs. Rem. Sens. 12 (11), 4672–4683.
Wang, Z., Gao, D., Lei, X., Wang, D., Gao, J., 2020. Machine learning-based seismic spectral attribute analysis to delineate a tight-sand reservoir in the Sulige gas field of central Ordos Basin, western China. Mar. Petrol. Geol. 113, 104136.
Xue, Ya-juan, Cao, Jun-xing, Du, Hao-kun, Lin, Kai, Yao, Yao, 2016a. Seismic attenuation estimation using a complete ensemble empirical mode decomposition-based method. Mar. Petrol. Geol. 71, 296–309.
Xue, Y.J., Cao, J.X., Tian, R.F., Du, H.K., Yao, Y., 2016b. Wavelet-based cepstrum decomposition of seismic data and its application in hydrocarbon detection. Geophys. Prospect. 64 (6), 1441–1453.
Xue, Y.J., Cao, J.X., Wang, X.J., Li, Y.X., Du, J., 2019. Recent developments in local wave decomposition methods for understanding seismic data: application to seismic interpretation. Surv. Geophys. 40 (5), 1185–1210.
Zolotukhin, A.B., Gayubov, A.T., 2019, November. Machine learning in reservoir permeability prediction and modelling of fluid flow in porous media, 700(1. In: IOP Conference Series: Materials Science and Engineering. IOP Publishing, 012023.
Zhang, Q., Wei, C., Wang, Y., Du, S., Zhou, Y., Song, H., 2019. Potential for prediction of water saturation distribution in reservoirs utilizing machine learning methods. Energies 12 (19), 3597.